J Musculoskelet Neuronal Interact 2008; 8(4):401-409

Original Article

Hylonome

Strength indices from pQCT imaging predict up to 85% of variance in bone failure properties at tibial epiphysis and diaphysis

S.A. Kontulainen[1], J.D. Johnston[2], D. Liu[2], C. Leung[2], T.R. Oxland[2], H.A. McKay[2,3]

[1]College of Kinesiology, University of Saskatchewan, Saskatoon, SK, Canada; [2]Division of Orthopaedic Engineering Research, University of British Columbia, Vancouver, BC, Canada; [3]Center of Hip Health, Vancouver, BC, Canada

Abstract

Our primary objective was to validate the Bone Strength Index for compression (BSI_C) by determining the amount of variance in failure load and stiffness that was explained by BSI_C and bone properties at two distal sites in human cadaveric tibiae when tested in axial compression. Our secondary objective was to assess the variance in failure moment and flexural rigidity that was explained by bone properties, geometry and strength indices in the tibial diaphysis when tested in 4-point bending. Twenty cadaver tibiae pairs from 5 female and 5 male donors (mean age 74 yrs, SD 6 yrs) were measured at the distal epiphysis (4 and 10% sites of the tibial length from the distal end) and diaphysis (50 and 66% sites) by peripheral Quantitative Computed Tomography (pQCT; XCT 2000, Stratec). After imaging, we conducted axial compression tests on the distal tibia and 4-point bending tests on the diaphysis. Total bone mineral content and BSI_C (product of total area and squared density of the cross-section) at the 4% site predicted 75% and 85% of the variance in the failure load and 52% and 57% in stiffness, respectively. At the diaphyseal sites 80% or more of the variance in failure moment and/or flexural rigidity was predicted by total and cortical area and content, geometry and strength indices corresponding to the axes of bending.

Keywords: pQCT, Strength Indices, Failure Load, Stiffness, Moment, Flexural Rigidity

Introduction

Peripheral quantitative computed tomography (pQCT) provides measures of bone cross-section related to bone size (area), mass (mineral content), apparent tissue density and geometry (spatial distribution of mass). In addition, strength indices, which combine bone cross-sectional geometry and tissue density measures, are provided by pQCT manufacturer's software (XCT), or can be calculated by the operator. To date, experimental evidence of bone properties and strength indices that best represent whole bone failure characteristics in the human long bone is scarce. This is especially true at the tibial epiphysis and diaphysis, sites that are commonly assessed for bone loading, unloading and growth studies[1,2].

Estimating long bone strength with medical imaging presents a challenge. Bone's ability to resist different types of loading (axial compression, bending, torsion) is related to both size and distribution of the bone material within a cross-section (i.e., bone geometry) and the material properties of bone tissue (e.g., the elastic modulus which determines bone material's stiffness before yielding, and the micro-structural factors which affect the post-yield behaviour of bones). The geometry of diaphyseal bone that best resists loading from multiple directions is one where cortical bone mass is distributed at an optimal distance from the neutral axes to resist bending and torsional loads. The cross-sectional moment of inertia (CSMI) describes this distribution of material and is essentially a measure of how effectively the cross-section resists bending in the x- or y-plane ($CSMI_x$ $CSMI_y$) or torsional ($CSMI_p$ or J) loading[3]. The maximum bending stress that bone can resist prior to failure can be estimated using the Section Modulus (Z). Z is CSMI divided by the maximum distance from the periosteum to a particular bending (Z_x or Z_y) or torsional axis (Z_p)[4].

The authors have no conflict of interest.

Corresponding author: Saija Kontulainen, College of Kinesiology, University of Saskatchewan, 87 Campus Drive, Saskatoon, SK S7N5B2 Canada
E-mail: saija.kontulainen@usask.ca

Accepted 28 October 2008

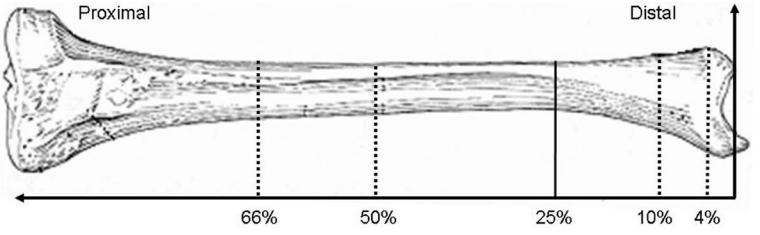

Figure 1. Scanning sites are shown with the dashed lines. The solid line points the 25% site where bone was cut to separate distal part for the compression test.

In regards to the material properties of bone tissue, the elastic modulus (E) is a measure of the stiffness of the bone material. E is dependent on the level of tissue mineralization and microstructure[5,6]. Although the elastic modulus of bone cannot be measured directly with currently available imaging techniques, pQCT-derived cortical bone's density has been used to estimate tissue mineralization[7], which is associated with elastic modulus[8,9]. Stratec software offers a bone strength index called Stress Strain or Stability Index (SSIx, SSIy and SSIp, mm^3). SSI is the product of Z and the ratio of measured cortical density (CoD) to physiologic bone density (1200 mg/cm^3)[10,11]. The predecessor to SSI was Bone Strength Index (BSI), which was the product of cortical bone CSMI and CoD[7]. In the rat femoral diaphysis, this classic BSIx predicted 87% of variance in failure load in 3-point bending[7]. Classic BSI has not yet been validated with mechanical testing of human long bone. However, SSI_p in the radial epi- and diaphysis was closely associated with failure load when loaded in 3-point bending[12,13]. and a loading configuration mimicking a fall on the outstretched arm[13-15]. The association between SSI and failure moment or structural rigidity (bending stiffness) in the human tibial diaphysis has not yet been reported.

At the long bone epiphyses, using any aforementioned strength indices would be inappropriate for two reasons. First, these indices are usually derived from cortical bone geometry, and thus, require accurate assessment of the cortical compartment. As the average cortical shell thickness at the epiphysis can be less than the pixel size used in clinical imaging (0.3 to 0.5 mm), pQCT is often incapable of accurately assessing cortical compartments at these sites[16,17]. Second, these indices assess resistance to bending and torsional loads which are common in the diaphysis; whereas the epiphysis is primarily loaded in axial compression[18]. To resist the compression stress transmitted from the large cartilage areas of the joint, the trabecular network at the epiphysis is conveniently aligned to absorb energy from impacts to the cortical shells[18,19]. In mechanical tests of isolated trabecular and cortical bone specimens, the trabecular or cortical density - compressive stress relationship was related to the square of the apparent density[20]. Based on this evidence, an index for bone strength (IBS or BSI_C) was proposed for whole vertebral bodies[21] and long bone ends[22]. To reflect both the bone size and material contributions to whole bone strength, BSIc is the product of total bone cross-sectional area (ToA) and the square of the total density (ToD). It is a simple reorganization of Hooke's Law: $(Stress=F/A)^4$. As ultimate compressive stress (F/ToA) is directly proportional to density squared (ToD^2)[20], force (F) is directly proportional to ToD^2*ToA. Thus, this model provides a non-invasive bone strength measure incorporating both bone material and its distribution. BSI_C is suited for sites primarily loaded in compression and has been used to assess the distal radius in unilateral loading[23] and the distal tibia in pediatric bone studies[24,25]. However, BSI_C has not yet been validated in the human long bone epiphysis.

Therefore, our primary objective was to validate BSI_C by determining the variance in compressive failure load and stiffness explained by bone properties and BSI_C at two distal epiphyseal sites in human cadaveric tibiae. Our secondary objective was to assess the variance in failure moment and flexural rigidity, explained by bone properties, cortical bone geometry and derived strength indices in the tibial diaphysis when tested in 4-point bending.

Methods

We obtained 20 fresh human cadaver tibiae from our institution's Department of Anatomy. Age at death of 5 female and 5 male donors ranged from 68 to 80 years (mean age 74, SD 6 years). All specimens were fresh frozen at -20°C and thawed for imaging and mechanical tests. This study was approved by the Clinical Ethics Review Board at the University of British Columbia.

pQCT acquisition

We acquired a single 2.3 mm slice at the 4, 10, 50, and 66% sites (of tibial length) proximal to the distal tibial endplate (Figure 1) using the Norland/Stratec pQCT (XCT 2000, Stratec Medizintechnik GmbH, Pforzheim, Germany). These sites were selected as they represent distal and diaphyseal bone sites. We used an in-plane pixel size of 0.20 mm by 0.20 mm and a scan speed of 10 mm/s. A 30 mm planar scout view over the joint line was acquired to define the anatomic reference line. All measurements were performed by a single investigator (DL).

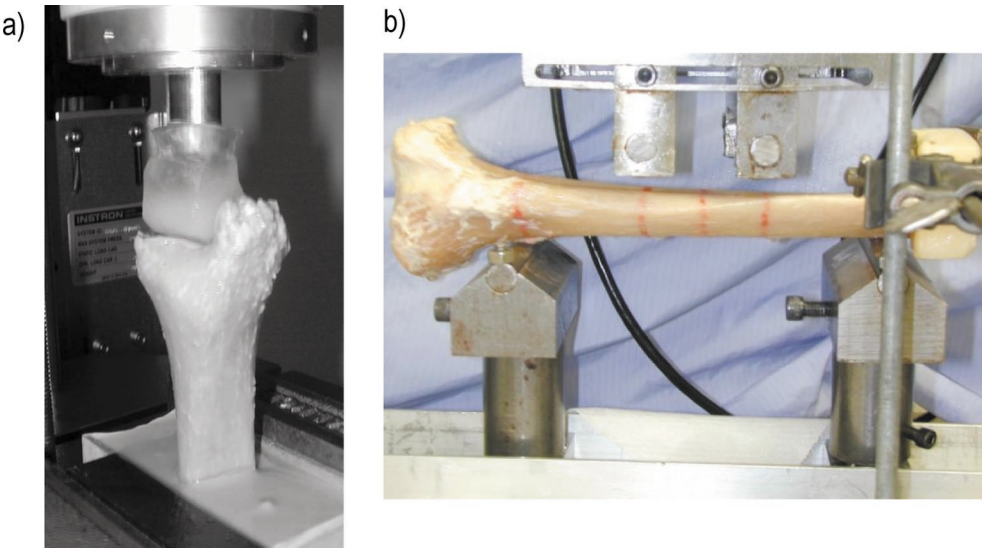

Figure 2. Mechanical test configurations: a) Compression; b) Four-point bending.

pQCT analysis

We used Norland/Stratec XCT 5.50 software for data analysis. At all measured sites we defined the periosteal (outer bone) boundary with a threshold of 169 mg/cm^3 using contour mode 3[26]. In other words, total bone area was the combined area of voxels with a density equal to or greater than 169 mg/cm^3. At the distal sites (4 and 10%), we used Peel mode 3 with a threshold of 480 mg/cm^3 to separate trabecular from cortical compartment (all voxels within the periosteal boundary with a threshold of equal to or less than 480 mg/cm^3 were defined as trabecular). At the distal site, the cortical compartment was defined by using separation mode 4 with an outer threshold of 169 mg/cm^3 and an inner threshold of 480 mg/cm^3. The diaphyseal cortex (50 and 66% sites) was defined using separation mode 4 with an outer threshold of 169 mg/cm^3 and an inner threshold of 710 mg/cm^3 [26]. Total, trabecular and cortical bone density was determined as the average density of those voxels used to define the total bone cross-section and the trabecular and cortical compartments, respectively.

pQCT outcomes

For the measured cross-section at the 4% and 10% sites, we obtained bone property measures for total bone and the cortical and trabecular compartments. These measures included area (ToA, CoA and TrA, mm^2); mineral content (ToC, CoC, and TrC, mg^2/mm); and apparent tissue mineral density (ToD, CoD and TrD, mg/cm^3). In addition, we calculated a bone strength index for compression (BSI_C, mg^2/cm^4) (see calculations below).

At the 50% and 66% sites, we obtained measures for total and the cortical compartment. These included cross-sectional area (ToA and CoA, mm^2); mineral content (ToC and CoC, mg^2/mm); and apparent total and cortical bone mineral density (ToD and CoD, mg/cm^3). We also determined two indices of bone geometry ($CSMI_y$ and Z_y) and two strength indices (BSI_y and SSI_y) in relation to the lateral or anteroposterior axis of bending, defined as the y-axis.

Strength indices were calculated using the following equations:

1. $BSI_C = ToD^2 \times ToA$
2. $CSMI_y = \Sigma(d_x^2 \times Av)$
3. $Z_y = \Sigma(d_x^2 \times Av)/d_{xmax}$
4. $BSI_y = \Sigma(d_x^2 \times Av) \times CoD$
5. $SSI_y = \Sigma(d_x^2 \times Av \times Dv/PCoD)/d_{xmax}$

d_x=distance from a cortical voxel to the x-axis; Av=area of the voxel; Dv=density of the voxel; CoD=cortical bone density; PCoD=estimated physiological "maximal" cortical bone density (1200 mg/cm^3).

Mechanical tests

After imaging, cadaveric tibiae were cut at the 25% site from the distal endplate with an EXAKT low speed diamond bandsaw. A servo-hydraulic materials testing machine (Model 8874, Instron Corp., Canton MA USA) was used for compression and bending tests.

In the compression test, the loading axis was aligned along the tibial longitudinal axis. A compressive force was applied to the distal plateau through a custom-fabricated PMMA indentor (Figure 2a). The test was conducted in displacement control to failure at a rate of 10 mm/s. Failure load (N) and stiffness (N/mm) were calculated from the load-displacement curve. Failure load was defined as the maximum load on the load-displacement curve. Stiffness was defined

as the slope of the load-displacement curve in the linear region located after the initial non-lineal toe region. The linear region for the stiffness calculation was identified by visual inspection, and confirmed by manually fitting a linear regression ($r^2>0.99$) to the load-displacement curve.

We performed four-point bending structural testing on the tibial diaphysis to determine the mechanical properties at the weakest point in the span between the 50% and 66% sites. We used a standardized test method (ASTM D790M-86)[27] with a custom designed 4-point bending fixture that employed a pivoting upper platen. The distal end of the cut specimens was embedded in a square PMMA pot for alignment purposes and to mimic the structural support provided by the removed distal plateau. The distal end of the specimen was free while the proximal medial end was placed upon a custom-made PMMA support to stabilize and prevent the specimen from rotating without medial-lateral constraint. The un-potted end of the specimen sat on a custom-made PMMA cup at the proximal side of the bottom support. Total lower span was on average three times the distance between the top supports. The ratio of the total span to the outer diameter in the lateral-medial direction was held constant (6:1). Load was applied directly to the 50% and 66% sites of the tibia (Figures 1 and 2b). The tibia was tested in the lateral-medial direction at a loading rate of 0.1mm/s. All tibiae were kept moist before and during the tests. Failure moment (Nm) was calculated with the equation: $M=(F*L)/6$ where M is the failure moment (Nm), F is the failure load (N), and L is the span of lower supports. To maintain a constant span:diameter ratio the lower span width (L) was changed for each individual specimen. Span width has a direct effect on stiffness measured from the slope of the load-displacement curve. For this reason, we calculated flexural rigidity (EI) using the equation $EI=(23/1296)*(p)*L^3$ where E is the elastic modulus, I the moment of inertia, and p the slope of the load-displacement curve (N/mm)[27]. Flexural rigidity is fundamentally a bending stiffness measure incorporating span width.

Statistical Analysis

We report mean and standard deviations (SD) for failure mechanics, bone properties, geometry and strength indices. To assess the ability of the independent variables (bone properties, geometry and strength indices) to predict the variance in the mechanical test variables (failure load, stiffness, failure moment and flexural rigidity) we performed linear regression analysis. To assess the fit of each of these univariate models we report coefficients of determination (R^2). Data were analyzed using SPSS statistical software (Windows 14.0, SPSS Inc., Chicago, IL, 2003).

Results

Compression testing (tibia epiphysis)

We determined the failure load data for 17 bones. One bone had a fracture before the test and two bones were tested at a slower loading rate and were excluded from the analysis. The average failure load was 8292 (SD 3010) N and mean stiffness was 3884 (1044) N/mm.

At the 4% site, ToC predicted 75% and ToD predicted 68% of the variance in failure load, whereas ToA predicted only 27% of the variance in failure load (Table 1). Cortical bone properties (CoA and CoC) and BSI_C predicted 85-88% of the variance in failure load (Table 1). Fifty-one to 57% of the variance in stiffness was explained by ToC, TrC and BSI_C (Table 1). At the 10% site, ToC predicted 53%, CoA and CoC 63-74%, and BSI_C 60% of the variance in failure load (Table 1). Again, the measured variables predicted less of the variance in stiffness; BSI_C offered the highest R^2 value (0.40) (Table 1). Overall, the measures at the 10% site seemed to predict less of the variance in both failure load and stiffness than variables at the 4% site (Table 1).

Bending (tibia diaphysis)

Failure moment and flexural rigidity were determined for all 20 specimens. The average failure moment was 138 (SD 42) N and mean flexural rigidity 2.9 (0.9) N/mm. Overall, all cross-sectional properties related to size, mass and geometry explained, on average, 70-80% of the variance in moment and rigidity (Table 2). At the 50% site, ToC, CoA, CoC, Z_y and SSI_y predicted 80% or more of the variance in failure moment (Table 2). Flexural rigidity was best predicted by ToA and CoA ($R^2=0.80$). At the 66% site, greater than 80% of the variance in failure moment was predicted by ToC, CoA, CoC, Z_y and SSI_y (Table 2). The variance in flexural rigidity was best predicted by $CSMI_y$ and BSI_y ($R^2=0.80$). At both diaphyseal sites, CoD was not a significant predictor of the variance in failure properties. Further, density-weighting the bone geometry variables did not improve the prediction of moment or rigidity (Table 2).

Discussion

We aimed to validate BSI_C by determining the amount of variance in failure load and stiffness explained by BSI_C. We compared this to the variance explained by bone properties (size, content and density) measured at two sites of the distal tibiae. BSI_C measured at the 4% site from the distal plateau predicted 85% of the variance in failure load and 57% of the variance in stiffness, when loaded in compression. ToA, ToC and ToD at the same site predicted 27%, 75% and 68%, respectively, of the variance in failure load and 32-40% of the variance in stiffness. When these variables were measured at the 10% site, their ability to predict the variance in both failure load and stiffness seemed to be less than at the 4% site. If the 4% site experienced more local deformation when loaded to failure than the 10% site this could explain the more robust prediction equation at the ultradistal site.

Similar to BSI_C and total content, cortical bone content and area explained 87-88% of the variance in failure load. However, since the ability of pQCT to measure the thin corti-

4%	Mean	SD	R^2_{load}	Sig.[b]	$R^2_{stiffness}$	Sig.[b]
Total bone						
ToA	1372.6	216.6	0.27	*	0.40	*
ToC	303.4	97.4	0.75	*	0.52	*
ToD	218.6	48.7	0.68	*	0.32	*
Cortical bone						
CoA	107.6	41.7	0.88	*	0.48	*
CoC	53.9	26.3	0.87	*	0.52	*
CoWT	0.9	0.3	0.78	*	0.37	*
Trabecular bone						
TrA	1186.1	194.6	0.10	*	0.22	*
TrC	246.1	62.5	0.54	*	0.51	*
TrD	206.7	34.9	0.56	*	0.33	*
Strength index						
BSI_c	7217.2	3628.7	0.85	*	0.57	*
10%						
Total bone						
ToA	612.9	100.4	0.22	*	0.32	*
ToC	202.0	54.3	0.53	*	0.36	*
ToD	328.6	64.9	0.35	*	0.12	*
Cortical bone						
CoA	172.7	45.2	0.63	*	0.33	*
CoC	142.5	42.0	0.74	*	0.37	*
CoWT	2.1	0.5	0.57	*	0.17	*
CoD	820.5	47.6	0.42	*	0.16	*
Trabecular bone						
TrA	464.9	89.8	0.02	NS	0.13	*
TrC	69.4	25.8	0.04	NS	0.10	NS
TrD	148.0	38.9	0.06	NS	0.03	NS
Strength index						
BSI_c	7140.0	2687.1	0.60	*	0.40	*

[b]Significance, *p<0.05*

Table 1. Bone properties and BSI_C (mean, SD) at 4% and 10% sites and their coefficients of determination (R^2) with failure load and stiffness in compression test.

cal shell is limited by its resolution we recommend caution when interpreting results in the cortical compartment. At the 4% site, when we used an algorithm that presumes a circular cortical ring, the estimated average cortical wall thickness varied from 0.6 to 1.5 mm among our specimens. We used a pixel size of 0.2*0.2 mm, which may have provided enough resolution to assess thin cortical bone properties. Prevrhal and collegues[28] found that helical CT accurately measured cortical thickness down to 0.7 mm with a pixel size of 0.1*0.1mm. However, the accuracy of pQCT-derived cortical area or cortical wall thickness at the thin epiphyseal bone has not yet been examined. Resolution in clinical pQCT studies usually varies from 0.3 to 0.6 mm. Thus, cortical bone measurements at the distal tibia may be unreliable, especially at the ultradistal radius. For the clinical assessment of bone strength at the long bone ends, reporting BSI_C or ToC is better justified than using variables derived from a thin cortical shell.

Reporting BSI_C at the long bone epiphysis is also justified for other reasons. First, as ultimate compressive stress (F/ToA) is directly proportional to the square of ToD[20], force (F) is directly proportional to ToD^2 x ToA. ToD is considered to represent the apparent density of the bone cross-section as it includes both the material density of trabecular bone tissue and voids filled with marrow (porosity). The contribution of ToD to BSI_C is more pronounced (i.e., ToD is squared) and this implies that BSI is an index of relative

50%	Mean	SD	R^2_{moment}	Sig.[b]	$R^2_{ridigity}$	Sig.[b]
Total bone						
ToA	457.4	78.9	0.71	*	0.80	*
ToBMC	335.7	72.3	0.81	*	0.78	*
Cortical bone						
CoA	277.5	57.8	0.86	*	0.80	*
CoC	314.0	67.8	0.83	*	0.78	*
CoWT	4.5	0.8	0.68	*	0.52	*
CoD	1130.6	26.1	0.03	NS	0.04	NS
Geometry						
$CSMI_y$	11636.6	4503.0	0.70	*	0.67	*
Z_y	928.4	262.8	0.80	*	0.78	*
Strength indices						
BSI_y	13160.3	5077.6	0.71	*	0.68	*
SSI_y	1994.6	511.0	0.80	*	0.76	*
66%						
Total bone						
ToA	558.1	115.6	0.54	*	0.70	*
ToBMC	344.8	80.5	0.78	*	0.76	*
Cortical bone						
CoA	278.9	64.6	0.80	*	0.73	*
CoBMC	308.2	73.3	0.80	*	0.71	*
CoWT	3.9	0.7	0.62	*	0.43	*
CoD	1103.7	25.7	0.08	NS	0.03	NS
Geometry						
$CSMI_y$	14170.3	5873.1	0.77	*	0.80	*
Z_y	1057.1	339.2	0.77	*	0.78	*
Strength indices						
BSI_{By}	15661.7	6510.5	0.78	*	0.80	*
SSI_y	2360.4	717.1	0.76	*	0.77	*

[b]Significance, *p<0.05*

Table 2. Bone properties, geometry and strength indices (mean, SD) at 50% and 66% sites and their coefficients of determination (R^2) with failure moment and rigidity in bending test.

bone strength rather than of absolute bone strength[22]. Second, the BSI_C equation (ToD^2 x ToA) also represents the volumetric expression of mineral content multiplied by a volumetric mineral density (ToC^2/ToA=ToC x ToD). In other words, BSI_C captures the important contribution of bone mineral mass to bone strength. Although ToC explained 75% and ToD explained 68% of the variance in failure load, BSI_C explained 85%. We were underpowered to quantify the significance of these percentages due to the small number of specimens. However, in previous studies that assessed predictors of failure load at the distal radius, ToC at the 4% radius site predicted 45 to 81% of the variance in failure load in the loading configuration simulating a fall on the outstretched arm[13-15]. Similarly, radial ToC differentiated wrist fractured from non-fractured individuals[29]. Future studies with more specimens are needed to assess the ability of BSI_C to predict failure and fracture at the distal radius.

At both diaphyseal sites, the best predictors (ToC, CoA, CoC, Z_y and SSI_y) explained 70-86% of the variance in failure moment and rigidity. However, CoD was not associated with the mechanical properties we assessed. Interestingly, bone cross-sectional area, geometry and strength indices tended to be smaller at the mid-diaphysis compared with the 66% site, suggesting that the mid-diaphysis is relatively

weaker than the 66% site. However, as the variance explained by bone properties at both sites was similar, either site would provide an adequate assessment of bone strength in bending in the anterior-posterior plane at the tibial diaphysis. We chose to load the tibiae in this direction to test the diaphysis in its weakest direction, in which fractures often occur[30,31], and perpendicular to the bending plane during normal locomotion. As bone geometry and mechanical properties of the material are tuned to the loading direction results may have differed if bones were tested in the A-P bending[32].

Density-weighting of Z_y did not improve the prediction of failure moment or rigidity. In our specimens average cortical density values at the diaphysis varied only slightly. Thus, multiplying section modulus with a value that represented the ratio of cortical density to physiological density remained approximately constant. Therefore it is likely that this constancy explains the similar coefficients of determination we observed for SSI_y and Z_y at the tibial shaft. On the other hand, the influence of CoD on mechanical data may be a factor in subjects who have greater variability in cortical porosity or tissue mineralization such as growing children, patients with a disease or taking medications that affect bone metabolism. CoD values also vary across the cortex radially[33,34] and regionally[35,36], possibly reflecting the difference in tissue porosity[37] and mineralization[38]. Variability in CoD may challenge the selection of an appropriate threshold used to identify cortical bone boundaries and accurate definition of the cortical compartment.

There are several technical issues related to our design that are of note. First, our intent was to link mechanical to tomographical data rather than to translate findings to clinical outcomes. Despite this, mechanical tests were designed to be as clinically relevant as possible. Fracture of the tibial plafond occurs when the talus is driven into the tibia from axial compression[39]. To represent this, we used individual, custom-made PMMA pads to mimic the talus, and loaded the tibial plafond at a relatively fast displacement rate (10 mm/s). The PMMA indentor was used to distribute the applied compressive load at the distal tibial surface to minimize localized loading. However, it is possible that this distributed loading produced off-axis compressive loading and introduced bending, torsional and shear loads at the distal tibia. Materials often fail in shear when subjected to compressive loading[40]. Distal tibial (Pilon) fractures result from a combination of axial and rotational forces[39,41]. Thus, relating compressive failure load to imaged variables might have oversimplified the true loading condition. Further, there is a high degree of geometric heterogeneity along the longitudinal axis of the distal tibia, especially where the wide epiphysis narrows to the metaphysis. Due to this variation in bone shape, compressive loading is not uniform and failure may occur at localized sites and in planes oblique to the axis of loading. This is problematic as we related failure load and stiffness to specific geometric properties taken from a few sites aligned perpendicular to the axis of loading. The actual failure might have occurred in either or none of the measured sites. As a result, the load experienced at failure may not have adequately represented the failure load that each measured site was capable of withstanding. The 4 and 10% sites were chosen as they have relatively thin and thick cortical compartments, respectively. Therefore, they should provide comparable values to (hypothetical) measures at the precise failure site. It seems logical that failure would occur near the distal joint surface at the site closest to the loaded site. The loaded site is most likely to experience local stress concentrations that result in cracking and failure. This likelihood was supported by evidence in our study in that the coefficients of determination tended to be greater at the 4% site compared with the 10% site.

Similarly, the exact site of failure in four-point bending was not determined nor was this exact region of interest scanned prior to testing. Previous studies assessed the strength indices that best predicted failure in 3-point bending in human radii[23], rat[7] and mouse femurs[42], and goat humerii and femurs[43]. A three-point bending configuration enables a more direct comparison between bone and failure properties as the specific site that is scanned can be loaded to failure. However, 3-point bending imposes both bending and shear stresses at the fracture site. As tibial diaphysis fractures are often the result of bending[30], we chose to use a 4-point bending configuration to create a uniform bending moment between the 50% and 66% sites. Tibial structure across this region is relatively consistent. Thus, it is likely that the sites imaged provided a reasonable estimate of the mechanical properties in the region between the 50% and 66% sites. That said, the uniform bending moment we applied may have oversimplified the actual context in which fractures occur at the tibial diaphysis where both bending and torsional forces are experienced[3]. Finally, the obvious dampening effects of soft tissue, muscle mass and tone on the loads applied to the tibial tissue were not captured in our model.

Summary

BSI_C, which combines total area and the square of total density of the bone cross-section at distal tibia, provides a reasonable estimate of bone's resistance to compression at the distal tibia. In addition, bone mineral content of the total and cortical cross-sections provided a means to robustly predict bone failure in compression at the distal tibia. Strength indices related to cortical bone area, content and geometry (Z_y and SSI_y) were also strong predictors of bending strength at the tibial diaphysis.

Acknowledgements

Financial support to conduct the study was provided by the Canadian Institutes of Health Research. Dr. McKay is a Michael Smith Foundation for Health Research (MSFHR) Senior Scholar and Dr. Kontulainen was supported by a MSFHR postdoctoral award.

References

1. Ashe MC, Fehling P, Eng JJ, Khan KM, McKay HA. Bone geometric response to chronic disuse following stroke: a pQCT study. J Musculoskelet Neuronal Interact 2006;6:226-33.
2. Macdonald HM, Kontulainen SA, Khan KM, McKay HA. Is a school-based physical activity intervention effective for increasing tibial bone strength in boys and girls? J Bone Miner Res 2007;22:434-46.
3. Ferretti JL. Perspectives of pQCT technology associated to biomechanical studies in skeletal research employing rat models. Bone 1995;17(Suppl.):353S-64S.
4. Beer F, Johnston ER, Dewolf JT. Mechanics of Materials: 2nd edition. Canada: John Wiley & Sons; 1999.
5. Choi K, Kuhn JL, Ciarelli MJ, Goldstein SA. The elastic moduli of human subchondral, trabecular, and cortical bone tissue and the size-dependency of cortical bone modulus. J Biomech 1990;23:1103-13.
6. Martin RB. Determinants of the mechanical properties of bones. J Biomech 1991;24 (Suppl.1):79-88.
7. Ferretti JL, Capozza RF, Zanchetta JR. Mechanical validation of a tomographic (pQCT) index for noninvasive estimation of rat femur bending strength. Bone 1996;18:97-102.
8. Currey JD. The mechanical consequences of variation in the mineral content of bone. J Biomech 1969;2:1-11.
9. Currey JD. The effect of porosity and mineral content on the Young's modulus of elasticity of compact bone. J Biomech 1988;21:131-9.
10. Stratec. XCT 2000 Manual Software Version 5.50, http://www.stratec-med.com/literatur/manuals/man55e.pdf
11. Schiessl H, Ferretti, JL, Tysarczyk-Niemeyer G, Willnecker J. Noninvasive bone strength index as analyzed by peripheral quantitative computed tomography (pQCT). In: Schonau E, editor. Pediatric Osteology. Amsterdam: Elsevier; 1996. p. 141-5.
12. Wilhelm G, Felsenberg D, Bogusch G. Biomechanical examinations for validation of the Bone Strength-Strain Index SSI, calculated by peripheral quantitative computed tomography. In: Lyrithis GP, editor. Musculoskeletal Interactions. Vol II. Athens: Hylonome 1999: p. 105-11.
13. Lochmuller EM, Lill CA, Kuhn V, Schneider E, Eckstein F. Radius bone strength in bending, compression, and falling and its correlation with clinical densitometry at multiple sites. J Bone Miner Res 2002;17:1629-38.
14. Ashe MC, Khan KM, Kontulainen SA, Guy P, Liu D, Beck TJ, McKay HA. Accuracy of pQCT for evaluating the aged human radius: an ashing, histomorphometry and failure load investigation. Osteoporos Int 2006; 17:1241-51.
15. Muller ME, Webber CE, Bouxsein ML. Predicting the failure load of the distal radius. Osteoporos Int 2003;14:345-52.
16. Hangartner TN, Gilsanz V. Evaluation of cortical bone by computed tomography. J Bone Miner Res 1996; 11:1518-25.
17. Augat P, Gordon CL, Lang TF, Iida H, Genant HK. Accuracy of cortical and trabecular bone measurements with peripheral quantitative computed tomography (pQCT). Phys Med Biol 1998;43:2873-83.
18. Hayes W, Bouxsein ML. Biomechanics of cortical and trabecular bone: implications for assessment of fracture risk. Basic Orthopaedic Biomechanics. Philadephia: Lippincott-Raven Publishers; 1997.
19. Currey JD. Bones: Structure and Mechanics: Princeton University Press; 2002.
20. Carter DR, Hayes WC. Bone compressive strength: the influence of density and strain rate. Science 1976;194:1174-6.
21. Carter DR, Bouxsein ML, Marcus R. New approaches for interpreting projected bone densitometry data. J Bone Miner Res 1992;7:137-45.
22. Sievanen H, Kannus P, Nieminen V, Heinonen A, Oja P, Vuori I. Estimation of various mechanical characteristics of human bones using dual energy X-ray absorptiometry: methodology and precision. Bone 1996; 18(Suppl.1):17S-27S.
23. Kontulainen S, Sievanen H, Kannus P, Pasanen M, Vuori I. Effect of long-term impact-loading on mass, size, and estimated strength of humerus and radius of female racquet-sports players: a peripheral quantitative computed tomography study between young and old starters and controls. J Bone Miner Res 2003;18:352-9.
24. Macdonald H, Kontulainen S, Petit M, Janssen P, McKay H. Bone strength and its determinants in pre- and early pubertal boys and girls. Bone 2006;39:598-608.
25. Wetzsteon RJ, Petit MA, Macdonald HM, Highes JM, Beck TJ, McKay HA. Bone structure and volumetric BMD in overweight children: a longitudinal study. J Bone Miner Res 2008;23:1946-53.
26. Kontulainen S, Liu D, Manske S, Jamieson M, Sievanen H, Mckay H. Analyzing bone geometry by peripheral QCT and MRI: Comparison with bone histomorphometry. J Clin Densitom 2007;10:86-92.
27. ASTM D790M-86. Standard Test Methods for Flexural Properties of Unreinforced and Reinforced Plastics and Electrical Insulating Materials;1986.
28. Prevrhal S, Engelke K, Kalender WA. Accuracy limits for the determination of cortical width and density: the influence of object size and CT imaging parameters. Phys Med Biol 1999;44:751-64.
29. Schneider P, Reiners C, Cointry GR, Capozza RF, Ferretti JL. Bone quality parameters of the distal radius as assessed by pQCT in normal and fractured women. Osteoporos Int 2001;12:639-46.
30. Lenehan B, Fleming P, Walsh S, Kaar K. Tibial shaft fractures in amateur footballers. Br J Sports Med 2003;37:176-8.
31. Grutter R, Cordey J, Buhler M, Johner R, Regazzoni P.

The epidemiology of diaphyseal fractures of the tibia. Injury 2000;31(Suppl.3):C64-7.
32. Leppanen O, Sievanen H, Jokihaara J, Pajamaki I, Jarvinen TL. Three-point bending of rat femur in the mediolateral direction: introduction and validation of a novel biomechanical testing protocol. J Bone Miner Res Aug 2006;21:1231-7.
33. Kontulainen SA, Macdonald HM, McKay HA. Change in cortical bone density and its distribution differs between boys and girls during puberty. J Clin Endocrinol Metab 2006;91:2555-61.
34. Cheng S, Toivanen JA, Suominen H, Toivanen JT, Timonen J. Estimation of structural and geometrical properties of cortical bone by computerized tomography in 78-year-old women. J Bone Miner Res 1995;10:139-48.
35. Lai YM, Qin L, Hung VW, Chan KM. Regional differences in cortical bone mineral density in the weight-bearing long bone shaft -a pQCT study. Bone 2005; 36:465-71.
36. Nonaka K, Fukuda S, Aoki K, Yoshida T, Ohya K. Regional distinctions in cortical bone mineral density measured by pQCT can predict alterations in material property at the tibial diaphysis of the Cynomolgus monkey. Bone 2006;38:265-72.
37. Bousson V, Bergot C, Meunier A, Barbot F, ZParlier-CuauC, Laval-Jeantet Am,Laredo JD. CT of the middiaphyseal femur: cortical bone mineral density and relation to porosity. Radiology 2000;217:179-87.
38. Goldman HM, Bromage TG, Boyde A, Thomas CD, Clement JG. Intrapopulation variability in mineralization density at the human femoral mid-shaft. J Anat 2003;203:243-55.
39. Bone LB. Fractures of the tibial plafond. The pilon fracture. Orthop Clin North Am 1987;18:95-104.
40. Turner CH, Burr DB. Basic biomechanical measurements of bone: a tutorial. Bone 1993;14:595-608.
41. Ruwe PA, Randall RL, Baumgaertner MR. Pilon fractures of the distal tibia. Orthop Rev 1993;22:987-96.
42. Jamsa T, Tuukkanen J, Jalovaara P. Femoral neck strength of mouse in two loading configurations: method evaluation and fracture characteristics. J Biomech 1998;31:723-9.
43. Siu WS, Qin L, Leung KS. pQCT bone strength index may serve as a better predictor than bone mineral density for long bone breaking strength. J Bone Miner Metab 2003;21:316-22.